A Modified Nonlinear Chirp Scaling Algorithm for Air-borne Ice Radar

Zhao Bo, Lang Shinan, Liu Xiaojun, Fang Guangyou
Key Laboratory of Electromagnetic Radiation and Sensing Technology, Institute of Electronics, Chinese Academy of Sciences, Beijing 100190, China

E-mail: bzhao@mail.ie.ac.cn

Abstract. In this paper, a modified nonlinear chirp scaling (MNLCS) algorithm for air-borne ice radar data is proposed. The spatial geometry based on the two-layer medium is analyzed for the studying of MNLCS. The algorithm can compensate the refraction effects and the propagation velocity changes in different mediums automatically, and can improve the focusing feature of the scatters. According to the model of echo signal, the phase compensation factors and realized steps of the algorithm are given. Numerical experiments are executed. The experimental results show the effectiveness of the proposed algorithm.

1. Introduction

Sea level rise is an important indicator of global climate change. Sea level has been arising at about 2mm annually since the end of the last century. The result of continued sea level rise can be devastating for the survival of human [1]. Due to the glacier has the characteristics of small attenuation to the radio wave, stratified structure and uniform property, electromagnetic method or radar technology becomes a prevalent technique in the field of glaciology research for the measurement of ice sheet thickness [2].

Synthetic aperture method for ice radar data processing can improve the signal to noise ratio and along-track resolution, and the method can suppress clutter. Therefore, the method has a wide range of applications in glacier thickness measurements [3,4,5]. However, the synthetic aperture of the traditional ice radar is achieved by matched filtering [3,4], which requires repeatedly to solve the distance between the imaging point with radar [5]; meanwhile, the inherent problems like huge amount of computation for matched filtering method request a fast imaging method. Nonlinear chirp scaling algorithm, containing the secondary compression (SRC) that changed linearly with distance, is applicable to a wide swath imaging [6]. Range migration correction can be achieved effectively without interpolation, and along-track compression in range-Doppler domain can be easily combined with motion compensation [7].

In paper [8], a modified nonlinear chirp scaling algorithm was proposed, the principal idea of which is to compensate the high order coupling in the two-dimensional frequency domain, leaving only the coupling term that can be processed by nonlinear chirp scaling. The modified algorithm can significantly improve the image quality. To solve the two-layer medium imaging problem for ice radar with large processing angle and low-frequency ultra wide band, based on the existing nonlinear chirp scaling algorithm, we propose an improved nonlinear chirp scaling algorithm. The proposed algorithm can automatically compensate the change of the refraction effect and the propagation velocity of the electromagnetic wave. Due to the completely compensation of range migration for the target in the

Content from this work may be used under the terms of the Creative Commons Attribution 3.0 licence. Any further distribution of this work must maintain attribution to the author(s) and the title of the work, journal citation and DOI.
Published under licence by IOP Publishing Ltd

reference distance, the image quality of the reference point or even the entire imaging region is tremendously improved. The algorithm needs only complex multiplication and Fourier transform, which improves the operations efficiency greatly. Based on the actual parameters of the radar, we simulated ice radar echo data, then, conducted imaging simulation for nine point target located in the center and edge of the scene to validate the effectiveness of the algorithm.

This paper is organized as follows. In Section 2, we establish a radar echo model to get radar echo signal. Section 3 shows the detailed steps of the proposed improved nonlinear chirp scaling algorithm. Point target simulation is employed to validate the proposed algorithm in Section 4. Finally, we present the concluding remarks in Section 5.

2. The model of radar echo

We can see in Figure 1., the radar does uniform linear motion along azimuth. In position $x = uh$, the radar transmits linear FM pulse $p(t) = rect(t/T_t)e^{jpK_pt^2}e^{jw_ct}$, with the center frequency of w_c , in which t and h represent the fast time and slow time respectively. Assumed that the ice is uniform, linear, lossless, isotropic medium, and recording the relative permittivity and permeability of the ice sheet as e_r and m_r , respectively, in which $m_r \approx 1$, l represents the horizontal position of the ice surface refraction point. According to Snell's law of refraction, we can obtained

$$\frac{x-l}{\sqrt{(x-l)^2+H^2}} = \sqrt{e_r}\frac{l}{\sqrt{l^2+d^2}} \tag{1}$$

Arrange formula(1), we can get a quartic equation about l

$$l^4 - 2xl^3 + (x^2 + \frac{d^2 - e_rH^2}{1-e_r})l^2 - \frac{2xd^2}{1-e_r}l + \frac{x^2d^2}{1-e_r} = 0 \tag{2}$$

Taking into account the difference of electromagnetic waves propagation velocity between ice-medium and air, the equivalent distance between the carrier aircraft and the target can be respect as:

$$R(h;d) = R_{air}(h;d) + n_{ice}R_{ice}(h;d) \tag{3}$$

in which $n_{ice} = \sqrt{e_r}$ is the refractive index of the ice sheet.

Changing the received echo signal through digital down conversion in a quadrature mixer and low-pass filtering, we get:

$$s_0(t,h) = rect(\frac{uh}{L})rect(\frac{t-2R(h;d)/c}{T}) \times e^{jpK_p(t-2R(h;d)/c)^2}e^{-j2w_cR(h;d)/c} \tag{4}$$

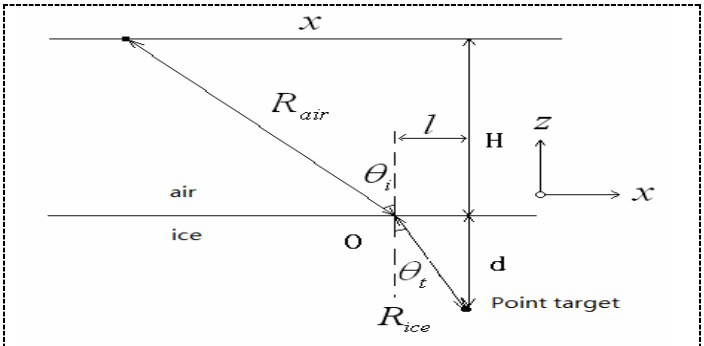

Figure 1. Electromagnetic wave propagation model.

3. Nonlinear Chirp Scaling algorithm

3.1. The Fourier transform of range and azimuth direction

According to the stationary phase principle, the frequency spectrum of echo signal in the wave number domain obtained by two-dimensional Fourier transform can be represented as:

$$S_0(k_z,k_x)=\exp\left(-jH\sqrt{(k_c+k_z)^2-k_x^2}\right)\times\exp\left(-jj\,(k_z,k_x;d)-j\frac{k_z^2}{2K}\right) \tag{5}$$

in which: k_z represents the wave number of the baseband, k_x represents the along-track wavenumber, k_c represents the number of carrier wave, K represents the frequency modulated rate of the signal in the wave number domain. Phase factor $j\,(k_z,k_x;d)$ can be expressed as:

$$j\,(k_z,k_x;d)=n_{ice}d\sqrt{(k_c+k_z)^2-(k_x/n_{ice})^2} \tag{6}$$

Using the Taylor series, the formula (6) can expand as polynomials:

$$j\,(k_z,k_x;d)=n_{ice}d(D(k_x)k_c+\frac{k_c}{D(k_x)}\frac{k_z}{k_c}-\frac{k_x^2}{2D^3(k_x)n_{ice}^2k_c}(\frac{k_z}{k_c})^2+\frac{k_x^2}{2D^5(k_x)n_{ice}^2k_c}(\frac{k_z}{k_c})^3+...) \tag{7}$$

in which

$$D(k_x)=\sqrt{1-(\frac{k_x}{k_cn_{ice}})^2} \tag{8}$$

3.2. The two-dimensional frequency compensation of reference point

The phase of the reference point for the signal can be completely compensated in the two-dimensional frequency domain, and the compensation function is:

$$\begin{aligned}H_1(k_z,k_x)=\exp\{&j(n_{ice}d_{ref}\sqrt{(k_c+k_z)^2-(k_x/n_{ice})^2}+jH\sqrt{(k_c+k_z)^2-k_x^2}\\&-jn_{ice}d_{ref}[D(k_x)k_c+\frac{k_c}{D(k_x)}\frac{k_z}{k_c}-\frac{k_x^2}{2D^3(k_x)n_{ice}^2k_c}(\frac{k_z}{k_c})^2]\}\end{aligned} \tag{9}$$

Here, the third and larger than third phase of the reference point is compensated. In the case of large processing angle, the remaining cubic phase error of the target far away from the reference point is big, which need to be compensated. The cubic phase compensation function is:

$$H_2(k_z,k_x)=\exp(j\frac{1}{3}Y(k_x)k_z^3) \tag{10}$$

and the two-dimensional frequency spectrum of the compensated signal can be expressed as:

$$S_1(k_z,k_x)=\exp(-jn_{ice}d(D(k_x)k_c+\frac{k_z}{D(k_x)}))\times\exp(-j\frac{k_z^2}{2K_m(k_x;d)}+j\frac{1}{3}Y(k_x)k_z^3) \tag{11}$$

in which:

$$\frac{1}{K_m(k_x;d)}=\frac{1}{K}-\frac{k_x^2d}{D^3(k_x)n_{ice}k_c^3} \tag{12}$$

Nonlinear CS algorithm considered changes of the frequency modulated rate in characteristics with the range direction d .The first order linear approximation for the space frequency modulated rate shown in formula (12) is:

$$K_m(k_x;d)\approx K_m(k_x;d_{ref})+K_{m1}(k_x)n_{ice}(d-d_{ref}) \tag{13}$$

in which:

$$K_{m1}(k_x)=\frac{k_x^2K_m^2(k_x;d_{ref})}{D^3(k_x)n_{ice}^2k_c^3} \tag{14}$$

3.3. The range direction inverse Fourier transforms

If $Y(k_x)$ is little enough, stationary phase points can be considered the same as the stationary phase points without cubic phase compensation, so the signal transformed to the range-Doppler domain can be represented as:

$$s_2(z,k_x)=\exp(-jD(k_x)k_c n_{ice}d)\exp[j\frac{1}{2}K_m(k_x;d)(z-\frac{n_{ice}d}{D(k_x)})^2]\exp\{j\frac{1}{3}Y(k_x)K_m^3(k_x;d)[z-\frac{n_{ice}d}{D(k_x)}]^3\} \quad (15)$$

3.4. Chirp Scaling

To control the changes of the frequency modulated rate with distance, the third CS function is introduced. Multiplying the corrected CS factor in the range-Doppler domain, we get:

$$H_3(k_x;d_{ref})=\exp\{j\frac{q_2(k_x)}{2}[z-\frac{n_{ice}d_{ref}}{D(k_x)}]^2+j\frac{q_3(k_x)}{3}[z-\frac{n_{ice}d_{ref}}{D(k_x)}]^3\} \quad (16)$$

3.5. Range compression, secondary range compression and range migration corrections

After the range direction inverse Fourier transforms, we transform the signal compensated by CS factor into two-dimensional frequency domain. In two-dimensional frequency domain, we represent the signal phase as k_z series, and expand each coefficient as $n_{ice}(d-d_{ref})$ series. In order to eliminate the migration item and secondary range compression item changed with distance, we set the coefficient of $n_{ice}(d-d_{ref})k_z$ to be 1, and the coefficient of $\left[n_{ice}(d-d_{ref})\right]^2 k_z$ and $n_{ice}(d-d_{ref})k_z^2$ to be 0. Then we can get:

$$Y(k_x)=\frac{K_{m1}(k_x)D(k_x)[2-D(k_x)]}{2K_m^3(k_x;d_{ref})[1-D(k_x)]} \quad (17)$$

$$q_2(k_x)=K_m(k_x;d_{ref})g(k_x) \quad (18)$$

$$q_3(k_x)=\frac{1}{2}K_{m1}(k_x)g(k_x)D(k_x) \quad (19)$$

in which

$$g(k_x)=\frac{1}{D(k_x)}-1 \quad (20)$$

After ignoring the higher-order terms, the phase function of signal in two-dimensional frequency domain can be represented as:

$$\begin{aligned}\angle S_3(k_z,k_x)=&-\frac{1}{2}\frac{1}{K_m(k_x;d_{ref})+q_2(k_x)}k_z^2-\frac{n_{ice}d_{ref}}{D(k_x)}k_z+\frac{1}{3}\frac{Y(k_x)K_m^3(k_x;d_{ref})+q_3(k_x)}{(K_m(k_x;d_{ref})+q_2(k_x))^3}k_z^3-n_{ice}(d-d_{ref})k_b\\&+\frac{1}{2}\frac{K_m(k_x;d_{ref})q_2(k_x)}{K_m(k_x;d_{ref})+q_2(k_x)}\times(\frac{n_{ice}(d_{ref}-d)}{D(k_x)})^2+\frac{1}{6}K_{m1}(k_x)g(k_x)D^2(k_x)\times(\frac{n_{ice}(d-d_{ref})}{D(k_x)})^3-D(k_x)k_c n_{ice}d\end{aligned} \quad (21)$$

The compensation function which has been done with range compression and range migration corrections can be represented as:

$$H_4(k_z,k_x)=\exp[j(\frac{1}{2}\frac{1}{K_m(k_x;d_{ref})+q_2(k_x)}k_z^2+\frac{n_{ice}d_{ref}}{D(k_x)}k_z-\frac{1}{3}\frac{Y(k_x)K_m^3(k_x;d_{ref})+q_3(k_x)}{(K_m(k_x;d_{ref})+q_2(k_x))^3}k_z^3)] \quad (22)$$

3.6. Along-track compression and residual phase compensation

The factors of azimuth focus and residual phase compensation can be represented as:

$$\begin{aligned}H_5(k_z,k_x)=&\exp(jD(k_x)k_c n_{ice}d)\times\exp(-\frac{j}{2}\frac{K_m(k_x;d_{ref})q_2(k_x)}{K_m(k_x;d_{ref})+q_2(k_x)}\times(\frac{n_{ice}(d_{ref}-d)}{D(k_x)})^2)\\&\times\exp[-j\frac{1}{6}K_{m1}(k_x)g(k_x)D^2(k_x)\times(\frac{n_{ice}(d-d_{ref})}{D(k_x)})^3]\end{aligned} \quad (23)$$

After doing along-track compression, residual phase compensation, and along-track inverse Fourier transform, we will get the final radar image.

We have shown the nonlinear chirp scaling imaging algorithm for high resolution ice radar above, and this algorithm can be extended easily from two layers of medium imaging to a multi-layer medium case, which need to make a corresponding modification for the compensation function.

4. Simulation results and analysis

In order to verify the validity of the nonlinear chirp scaling algorithm, we have done nine point targets array imaging simulation. In this simulation, the flight height H of radar carrier aircraft is 2000m, the flight speed u is 100m/s， and system coherent integration numbers(COH) is 64, The maximum Doppler frequency $2u/l$ of the target is 83.3Hz. According to the radar system parameters as shown in Table 1, we produce the point target echo data based on the formula (3), and the imaging results is shown in figure 2. There are nine point targets in the imaged scene, and the center point target is located in (0,-2000), and the remaining point targets distribute around the center point target with 500m equal interval. Taking the center point target and lower right point target (500, -2500) as an example for the detailed analysis of the imaging results, we give out the image of point target and the two dimensional compression curve after 8 times, as shown in Figure 3. The point targets image can be seen clearly from Figure 3, and the compression curve of range and azimuth is good.

Table 1. HRI-GPR system parameters

Parameters	**value**	**unit**
Radar Type	LFM pulse	---
RF carrier frequency	125	MHz
Transmitted pulse width	10	μs
Bandwidth	50	MHz
Sampling frequency	166.7	MHz
PRF	9.6	KHz
Antenna beamwidth in along-track direction	66	°

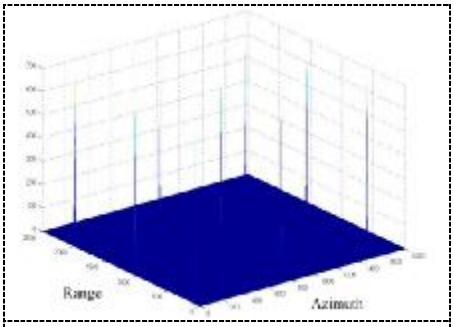

Figure 2. Nine point target imaging.

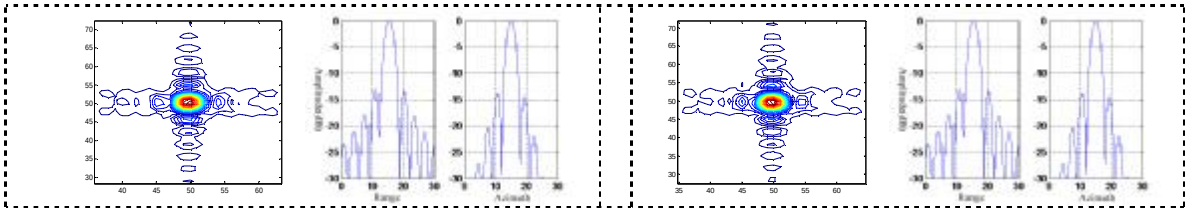

(a) Center point target. (b) Low right corner point target.

Figure 3. Point target imaging and Two-dimensional compression curve.

Table 2. Point target quality indicators and comparison

		Simulation value			theoretical value
		PSLR (dB)	ISLR (dB)	Resolution (m)	Resolution (m)
Central point	Range	-13.07	-10.23	2.66	2.65
	Azimuth	-13.79	-12.50	1.83	1.97
lower right corner point	Range	-12.93	-10.21	2.66	2.65
	Azimuth	-13.72	-12.58	1.92	2.15

Taking the point of top left, center and bottom right in the imaging scene as an example, Table 2 gives out the peak sidelobe ratio (PSLR), integral sidelobe ratio (ISLR) ,and the resolution of the distance and azimuth, and the values are compared with the theoretical value. Simulation peak sidelobe ratio and integrated sidelobe ratio are consistent with the theoretical values, and the resolution is close to the theoretical resolution given by literature [5], and indicators of point target response meet the

requirements. From table 2, the azimuth resolution gets lower and lower as the target depth increasing, which is due to the length of the synthetic aperture of all the point targets are same in our simulation, Doppler bandwidth generated by distant target is narrow, resulting to the resolution lower. For the closer target, the range resolution is relatively lower, which is because the range migration of closer target is larger. After the completion of the range migration correction, there is still a certain range bending. After the compression of azimuth, the range main lobe is broadening.

5. Conclusion

In this paper, based on the space geometric model and the echo signal form of high-resolution ice penetrating radar, we have derived an improved nonlinear chirp scaling algorithm which is suitable for nadir-looking synthetic aperture radar imaging, and we have given out the expressions of each compensation factor and the implementation steps of the algorithm. The proposed algorithm can automatically correct the change of the refraction effect in different medium interface and the propagation velocity in different medium for the electromagnetic wave without solving a quartic equation, and can effectively improve the performance of the focus of the scattering point, so it can be used for sectional imaging to ice penetrating radar. In this paper, two layers medium imaging is taken as an example, the algorithm can be easily extended to the case of multilayer medium. In simulation test, we analyze the imaging results, in which the image quality indicators of peak sidelobe ratio, the integral sidelobe ratio and resolution are consistent with the theoretical value. The experimental results show the effectiveness of the proposed algorithm.

6. Acknowledgment

This work is supported by the National Natural Science Foundation of China (grant No. 40976114) and the National High Technology Research and Development Program of China (863 Program No. 2011AA040202).

7. Reference

[1] S. Gogineni, T. Chuah, C. Allen, K. Jezek and R. K. Moore 1998 *J. Glaciol.* **44(148)** 659–669
[2] Justin J. Legarsky, Sivaprasad P. Gogineni, and Torry L. Akins 2001 *IEEE Trans. On Geosciences and Remote Sensing*. **39(10)** 2109-2117
[3] Matthew E. Peters, Donald D. Blankenship, Sasha P. Carter, Scott D. Kempf, Duncan A. Young, and John W. Holt 2007 *IEEE Trans. on Geosciences and Remote Sensing*. **45(9)** 2725-2736
[4] Florence Hélière, Chung-Chi Lin, Hugh Corr, David Vaughan 2007 *IEEE Trans. On Geosciences and Remote Sensing*. **45(8)** 2573-2582
[5] Davidson G W, Cumming I G, Ito M R 1996 *IEEE Trans. On Aerospace and Electronic Systems*. **32(1)** 121-133
[6] Ian G.Cumming, Frank H.Wong 2005 *Digital Processing Synthetic Aperture Radar Data* (London: Artech House)
[7] Liu Guangping 2003 *Efficient imaging generation for ultra-wide band synthetic aperture radar* (Changsha, Hunan: The National University of Defense Technology)